Supplementary Information

Tunable Squeeze-Activated GHz Acoustofluidics for Stable Trapping and Separation of Sub-100 nm Nanoparticles

Yiming Liu[a,1], Wei Wei[a,1], Hang Qi[a,1], Shuaihua Zhang[a], Yongqi Chen[a], Yaping Wang[a*], Xuexin Duan[a*]

[a] *State Key Laboratory of Precision Measuring Technology & Instruments, College of Precision Instrument and Opto-electronics Engineering, Tianjin University, Tianjin 300072, China*

[1] These authors contribute equally to this work.

* Corresponding author: xduan@tju.edu.cn (X. Duan).

* Corresponding author: wangyaping@tju.edu.cn (Y. Wang).

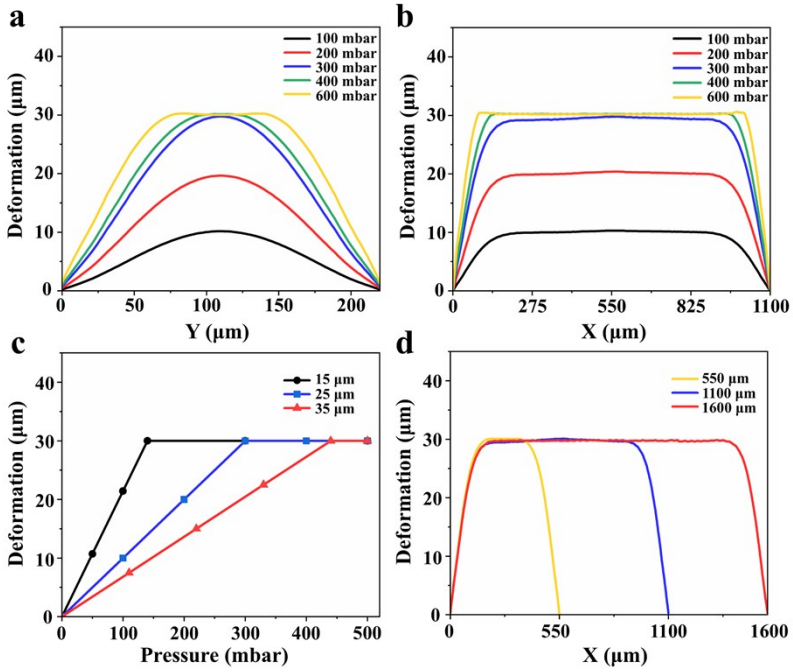

Fig. S1 For a fixed membrane thickness of 25 μm, the deformation curves at the maximum deformation points for **(a)** cross-sections perpendicular to the direction of liquid flow and for **(b)** cross-sections parallel to the direction of liquid flow under different pressures. Deformation conditions at the maximum deformation points under different **(c)** membrane thicknesses and **(d)** membrane lengths. The microchannel deformation exhibits a linear response to applied pressure up to 300 mbar, at which point the membrane contacts the channel bottom. Beyond this threshold, further pressure increases progressively reduce the residual channel height on both sides. Regarding membrane thickness, while thinner membranes offer higher deformability, they are prone to collapse during fabrication. Conversely, thicker membranes require excessive actuation pressure, increasing the risk of rupture. Consequently, a 25 μm thickness was selected to balance mechanical stability with operational feasibility. In terms of valve length, increasing the length extends the uniform deflection region, thereby enhancing the pre-enrichment effect. However, a length of 550 μm proved insufficient for effective pre-enrichment, whereas 1600 μm introduced structural instability due to potential collapse. Therefore, the valve length was optimized to ensure both efficient pre-enrichment and experimental stability.

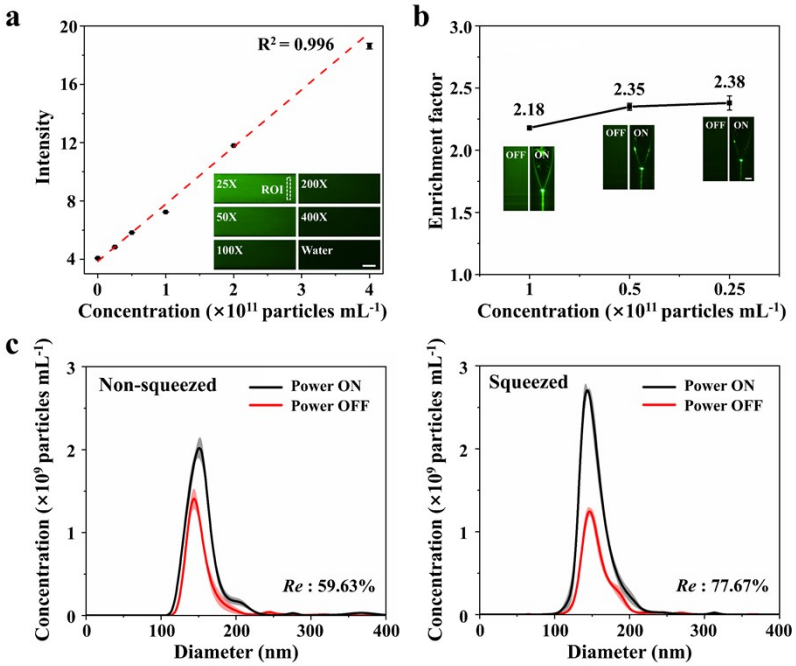

Fig. S2 (a) Calibration curve showing the relationship between the concentration of 150 nm polystyrene nanoparticles and fluorescence intensity. Scale bar, 100 μm. **(b)** Enrichment images and enrichment factors of nanoparticles at different concentrations. Scale bar, 50 μm. The inlet flow rate was set to 0.9 μL min^{-1}, the collection outlet flow rate was -0.3 μL min^{-1}, and the waste outlet flow rate was -0.6 μL min^{-1} (the negative sign indicates the pump is in suction mode). At nanoparticle concentrations of 1, 0.5, and 0.25 × 10^{11} particles mL^{-1}, the enrichment factors were 2.18, 2.35, and 2.38, respectively. "ON" and "OFF" refer to the BAW device power. **(c)** Comparison of the recovery efficiency (*Re*) of 150 nm nanoparticles under non-squeezed and squeezed conditions.

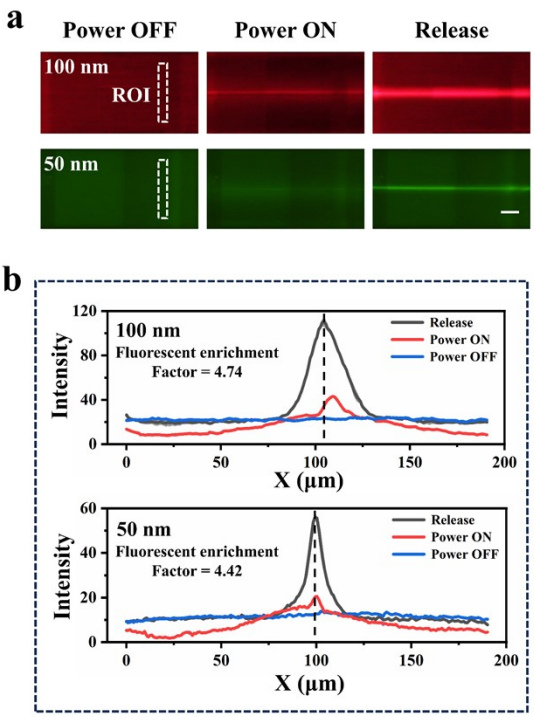

Fig. S3 (a) Fluorescence images of enriching and releasing 100 nm and 50 nm particles with an inlet flow rate of 0.6 μL min^{-1} under squeezed microchannel. Scale bar, 50 μm. **(b)** Image intensity analysis of the region of interest (ROI). Scale bar, 50 μm.

Table S1 Comparison of different nanoparticle manipulation techniques

Method	Limiting size	Recovery efficiency (%)	Throughput	Advantages	Disadvantages
Ultracentrifugation[1,2]	50 nm	2-80	3-12 h	Capability for large sample volumes	Expensive; Time-consuming
Ultrafiltration[1,2]	200 nm	10-80	0.5-3 h	Portable; Simple operation	Clogging; Particle damage
Viscoelastic Microfluidics[3]	20 nm	-	-	Relatively simple channel geometry; Down to 20 nm	Dependence on polymer additives; Low throughput
Dielectrophoretic Microfluidics[4]	50 nm	-	~30 min	High selectivity	Particle damage; Requirement for specific buffers
DLD Microfluidics[5]	110 nm	-	0.1-0.2 nL min^{-1}	Deterministic separation trajectories; High resolution	Clogging; Complex nanofabrication.
TSGA (this work)	50 nm	79	0.6-3 uL min^{-1}	Dynamic "on-demand" tunability; Continuous flow operation; High purity; Biocompatibility	Requirement for external pressure; Relative low throughput

Reference

1 F. Liu, O. Vermesh, V. Mani, T. J. Ge, S. J. Madsen, A. Sabour, E.-C. Hsu, G. Gowrishankar, M. Kanada, J. V Jokerst, R. G. Sierra, E. Chang, K. Lau, K. Sridhar, A. Bermudez, S. J. Pitteri, T. Stoyanova, R. Sinclair, V. S. Nair, S. S. Gambhir and U. Demirci, *ACS Nano*, 2017, **11**, 10712–10723.

2 F. A. W. Coumans, A. R. Brisson, E. I. Buzas, F. Dignat-George, E. E. E. Drees, S. El-Andaloussi, C. Emanueli, A. Gasecka, A. Hendrix, A. F. Hill, R. Lacroix, Y. Lee, T. G. van Leeuwen, N. Mackman, I. Mäger, J. P. Nolan, E. van der Pol, D. M. Pegtel, S. Sahoo, P. R. M. Siljander, G. Sturk, O. de Wever and R. Nieuwland, *Circ. Res.*, 2017, **120**, 1632–1648.

3 M. Asghari, X. Cao, B. Mateescu, D. van Leeuwen, M. K. Aslan, S. Stavrakis and A. J. deMello, *ACS Nano*, 2020, **14**, 422–433.

4 S. D. Ibsen, J. Wright, J. M. Lewis, S. Kim, S.-Y. Ko, J. Ong, S. Manouchehri, A. Vyas, J. Akers, C. C. Chen, B. S. Carter, S. C. Esener and M. J. Heller, *ACS Nano*, 2017, **11**, 6641–6651.

5 B. H. Wunsch, J. T. Smith, S. M. Gifford, C. Wang, M. Brink, R. L. Bruce, R. H. Austin, G. Stolovitzky and Y. Astier, *Nat. Nanotechnol.*, 2016, **11**, 936–940.